Generalized Inverse Participation Ratio as a Possible Measure of Localization for Interacting Systems

N. C. Murphy, R. Wortis, and W. A. Atkinson*
Department of Physics and Astronomy, Trent University, 1600 West Bank Dr., Peterborough ON, K9J 7B8, Canada
(Dated: April 18, 2011)

We test the usefulness of a generalized inverse participation ratio (GIPR) as a measure of Anderson localization. The GIPR differs from the usual inverse participation ratio in that it is constructed from the local density of states rather than the single-electron wavefunctions. This makes it suitable for application to many-body systems. We benchmark the GIPR by performing a finite-size scaling analysis of a disordered, noninteracting, three-dimensional tight-binding lattice. We find values for the critical disorder and critical exponents that are in agreement with published values.

PACS numbers: 71.23.An,71.55.Jv,72.15.Rn

I. INTRODUCTION

Anderson localization is a phenomenon in which quantum particles may be localized due to a random potential, even though the particles are classically unbound.[1] The theory for noninteracting particles is well-developed: in one and two dimensions, particles are localized by arbitrarily weak disorder, and in three dimensions states may be localized or extended depending on the strength of disorder.[2]

Most real particles are interacting, however, and there has been an ongoing effort to understand how interactions modify the noninteracting picture, either because of screening of the disorder potential, or because of loss of quantum coherence due to inelastic scattering.[3] Until recently, neither of these effects was believed sufficient to change the noninteracting picture at zero temperature. However, experiments[4] in two dimensional semiconductor films identified a zero-temperature metal-insulator transition (MIT) that appears to result from electron interactions.[5] More recently, it has been suggested that weakly-interacting one and two-dimensional systems will exhibit a finite-T Anderson MIT.[6,7]

There is also interest in Anderson localization in strongly interacting systems.[8] Many of the most interesting strongly correlated materials are insulators, but can have their electronic properties tuned by chemical doping. Of particular interest are materials, such as the high temperature superconductors, whose parent compounds have an interaction-driven Mott insulating phase. These materials become superconductors when doped with a few percent of electron or hole donor atoms, but pass through various intermediate phases in which disorder seems to play an important role. There is an abundancy of questions about how the electronic properties of these materials are modified by doping-related disorder. Of particular relevance to this work, there have been recent questions about how localization physics is altered near the Mott MIT,[9–14] and about the phase transition between the Anderson and Mott insulating phases.[15–17]

Finally, trapped atomic gases in random optical lattices have now been experimentally realized.[18–22] These systems are interesting because the strength of the atom-atom interactions can by tuned by application of an external magnetic field. There is therefore the prospect of making a controlled study of Anderson localization as a function of interaction strength.

Numerical calculations have played an important role in understanding Anderson localization in noninteracting systems. However, many of the techniques developed for measuring localization in noninteracting systems cannot be extended to interacting systems since they require knowledge of the *single-particle* eigenstates of the system and, with the exception of self-consistent field calculations, many-body wavefunctions cannot generally be written as a simple product of single-particle states. There is, therefore, an interest in developing new numerical methods for studying the Anderson MIT in interacting systems.

With this in mind, there have been several proposals that the localization transition can be detected by studying the statistical properties of the local density of states (LDOS) $\rho(\mathbf{r},\omega)$. The geometric average of the LDOS, $\rho_g(\omega)$, is an order parameter for the Anderson MIT in the limit of infinite system size[23,24] because it vanishes when the local spectrum is discrete. In infinite systems, this occurs only at energies at which the states are localized and not at which the states are extended. A generalization of dynamical mean field theory based on incorporating $\rho_g(\omega)$ into the self-consistency cycle was developed to study interacting disordered systems.[15,16,24] As a practical measure of localization in finite systems, however, $\rho_g(\omega)$ is problematic because the spectrum is always discrete, and this can obscure the Anderson MIT.[25,26] More recently, several groups have suggested that the Anderson transition can be detected by studying the distribution of $\rho(\mathbf{r},\omega)$ values,[16,27–29] and it has been shown that this distribution scales differently with system size for localized and delocalized states.[28]

In this work, we consider a quantity, the generalized inverse participation ratio (GIPR), that is related to the

LDOS via

$$G_2(\omega) = \frac{\sum_i \rho(\mathbf{r}_i,\omega)^2}{[\sum_i \rho(\mathbf{r}_i,\omega)]^2}. \quad (1)$$

Equation (1) is defined for a lattice, so that $\rho(\mathbf{r}_i,\omega)$ is the density of states projected onto the local Wannier orbital at the ith site of the lattice. The GIPR was used previously in finite size scaling studies,[13] but a careful examination of its scaling properties has not been made. This is the purpose of this paper.

The GIPR is analogous to the usual inverse participation ratio (IPR) for noninteracting systems,

$$I_{q,\alpha} = \frac{\sum_i |\Psi_\alpha(\mathbf{r}_i)|^{2q}}{[\sum_i |\Psi_\alpha(\mathbf{r}_i)|^2]^q}, \quad (2)$$

where $\Psi_\alpha(\mathbf{r}_i)$ is a single-particle wavefunction with quantum number α in the basis of Wannier orbitals. The IPR is conventionally defined with $q = 2$ and can be used to distinguish Anderson localized and extended states: for a finite d-dimensional system of linear size L, $I_{2,\alpha}$ satisfies

$$\lim_{L\to\infty} I_{2,\alpha} = \begin{cases} 1/L^d & \text{(extended states)} \\ \text{const.} & \text{(localized states)}, \end{cases} \quad (3)$$

for states that are far from the Anderson MIT, and exhibits multifractal scaling,[23,30–32]

$$\lim_{L\to\infty} I_{2,\alpha} = L^{-d_2}\tilde{F}[(W - W_c)L^{1/\nu}], \quad (4)$$

near the transition. Here, d_2 is the fractal dimension for $q = 2$, ν is a critical exponent, and W and W_c are the disorder and critical disorder strengths respectively.

For noninteracting systems, $G_2(\omega)$ reduces to the IPR when ω is equal to one of the eigenenergies of the system. This follows from substituting

$$\rho(\mathbf{r}_i,\omega) = \sum_\alpha |\Psi_\alpha(\mathbf{r}_i)|^2 \delta(\omega - E_\alpha), \quad (5)$$

into Eq. (1), where E_α are the discrete eigenenergies of the disordered lattice. However, for a general value of ω not equal to one of the eigenenergies, $G_2(\omega)$ is not well defined if the δ-functions in Eq. (5) are infinitely sharp, and the relationship between the IPR and the GIPR is therefore ambiguous. Moreover, we show below that if one broadens the δ-functions by an amount γ, there is no limiting value of γ in which the GIPR reduces to the IPR. The goal of this paper is to demonstrate that the GIPR can nonetheless be used to detect the Anderson MIT and to determine the critical parameters W_c, d_2 and ν.

We benchmark the GIPR by performing finite size scaling for a disordered noninteracting model, where the critical properties are well known. In Sec. II, we discuss how the broadening of the δ-functions in Eq. (5) is expected to affect the finite size scaling, and use this to select an optimal broadening. In Sec. III, we show the results of numerical finite size scaling, from which we extract values for the critical disorder and critical exponents at the Anderson MIT. We show that, with an appropriate choice for γ, it is possible to extract critical properties.

II. CALCULATIONS

The noninteracting Anderson model is

$$\hat{H} = -t\sum_{\langle i,j\rangle} |i\rangle\langle j| + \sum_i |i\rangle\epsilon_i\langle i|. \quad (6)$$

where $|i\rangle$ is the ket for a Wannier orbital at position i on the lattice and $\langle i,j\rangle$ indicates that the sum is over nearest-neighbour sites. The hopping matrix element is taken to be $t = 1$, and it therefore sets the energy scale, while the site energies ϵ_i are taken from a uniform distribution of random values ranging from $-W/2$ to $W/2$, where W is the strength of disorder. Calculations are performed for a three-dimensional ($d = 3$) cubic lattice of linear size L and with $N_s = L^3$ lattice points.

We use a recursion method[33] to find the local Green's function $G(\mathbf{r}_i,\omega+i\gamma)$ at site i, where γ is a small but finite shift off the real frequency axis. This method introduces an error through truncation of the recursion algorithm, and we have been careful to adjust the truncation criterion so that this error is much smaller than the error due to disorder averaging. The LDOS is given by the imaginary part of $G(\mathbf{r}_i,\omega + i\gamma)$. Formally, this is equivalent to

$$\rho_\gamma(\mathbf{r}_i,\omega) = \frac{1}{\pi}\sum_\alpha |\Psi_\alpha(\mathbf{r}_i)|^2 \frac{\gamma}{(\omega - E_\alpha)^2 + \gamma^2} \quad (7)$$

where E_α are the eigenenergies for a particular disorder realisation. Once $\rho_\gamma(\mathbf{r}_i,\omega)$ is known, the GIPR is calculated from Eq. (1). In this work, we focus on the band center ($\omega = 0$), where the Anderson transition is well-characterized. In particular, the Anderson MIT occurs at a critical disorder $W_c = 16.5t$ for the uniform disorder distribution used here.[34,35]

One of the main issues we face is how to choose γ. In the remainder of this section, we discuss how this choice affects both the LDOS and the scaling behavior of the GIPR. The relevant energy scale for comparison is the level spacing at the band center, $\Delta = 1/\rho_0 N_s$, where ρ_0 is the system-averaged density of states at $\omega = 0$. For strongly disordered systems, $\Delta \approx W/N_s$, while for weakly disordered systems, $\Delta \approx D/N_s$, where D is the bandwidth of the disorder-free lattice. For the cubic lattice considered here, the Anderson transition occurs at an intermediate disorder strength, so that Δ lies between these two limits.

Figure 1 shows the dependence of the LDOS on γ. When $\gamma \gtrsim \Delta$, the LDOS at ω is an average over states with $|\omega - E_\alpha| \lesssim \gamma$, with the consequence that the LDOS is more spatially uniform than the individual eigenstates making up the LDOS. Thus in Fig. 1, the sites A and B are spatially separated, and both have broad peaks at $\omega = 1$. It is not possible to tell, based on the LDOS for $\gamma = W/N_s$, whether these peaks indicate a single eigenstate or a cluster of eigenstates that happen to be close in energy. It is only when $\gamma \ll \Delta$ that we see that the local spectrum is quite different at the two sites

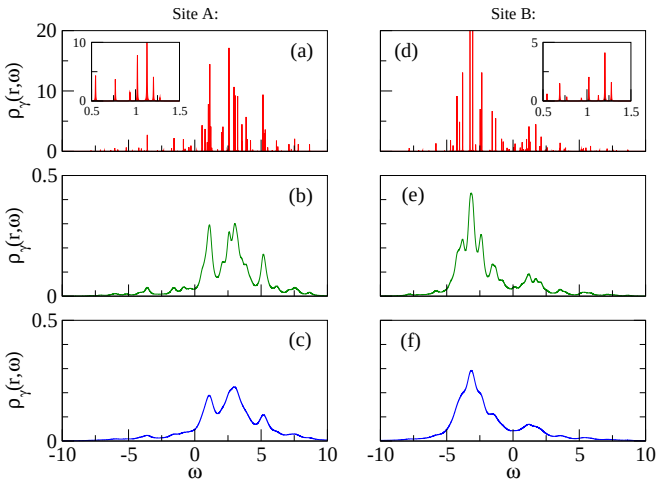

FIG. 1: (Color online) Local density of states for two well-separated lattice sites, "A" and "B", in a disordered lattice. Panels show the LDOS at (a)-(c) A and (d)-(f) B. All spectra are for the same configuration of disorder, but have different values of γ. Results are for (a), (d) $\gamma = 0.01W/N_s$; (b), (e) $\gamma = W/N_s$; (c), (f) $\gamma = 2W/N_s$, where the lattice has $N_s = 4^3$ sites and $W = 13$. Insets show expanded views of the LDOS near $\omega = 1$.

[Figs. 1(a) and (d)]. This suggests that the finite size scaling of the LDOS, and by extension the GIPR, should do a better job of distinguishing localized and extended states as γ is reduced.

However, the fact that the spectrum develops discrete peaks when $\gamma \ll \Delta$ does not mean that the LDOS samples only individual eigenstates in this limit. This is because most energies do not coincide with a peak. When $\gamma \ll \Delta$, the energy $\omega = 0$ lies in the tails of the surrounding peaks and Eq. (7) becomes

$$\rho_\gamma(\mathbf{r}_i, 0) = \frac{\gamma}{\pi} \sum_\alpha \frac{|\Psi_\alpha(\mathbf{r}_i)|^2}{E_\alpha^2}. \tag{8}$$

This means that even in the limit $\gamma \to 0$, $\rho(\mathbf{r}_i, 0)$ is averaged over a nonzero number of states. The LDOS at $\omega = 0$, and by extension the GIPR, does not change qualitatively when γ is reduced much below Δ.

We can learn more about the GIPR scaling by substituting Eq. (7) into Eq. (1), from which we obtain

$$G_2(0) \;=\; \sum_i \left(\sum_\alpha w_\alpha |\Psi_\alpha(\mathbf{r}_i)|^2 \right)^2 \tag{9}$$

where

$$w_\alpha = \frac{(E_\alpha^2 + \gamma^2)^{-1}}{\sum_\beta (E_\beta^2 + \gamma^2)^{-1}} \tag{10}$$

is a weighting factor satsifying $\sum_\alpha w_\alpha = 1$. In the limit of vanishing disorder, the wavefunctions are plane waves with $|\Psi_\alpha(\mathbf{r}_i)|^2 = N_s^{-1}$, and Eq. (9) gives $G_2(0) = N_s^{-1}$; this result is independent of γ and is identical to the scaling result for the IPR.

In the limit of large disorder, $W \gg W_c$, it is useful to rearrange Eq. (9) to obtain,

$$G_2(0) \;=\; \sum_\alpha w_\alpha^2 I_{2,\alpha} + \sum_{\alpha \neq \beta} w_\alpha w_\beta \sum_i |\Psi_\alpha(\mathbf{r}_i)|^2 |\Psi_\beta(\mathbf{r}_i)|^2. \tag{11}$$

The first term on the right hand side is a weighted sum of IPR values for eigenstates with $|E_\alpha| \lesssim \gamma$, while the second term consists of cross terms between pairs of eigenstates. The second term can be neglected when the distances between these localized states are large compared to the localization length ξ. We can estimate the typical distance between centers of localization of the states in Eq. (11) for the case $\gamma \gtrsim \Delta$. In this case, there are of order $2\gamma/\Delta$ states with $|E_\alpha| < \gamma$, and the mean separation of these is

$$\ell \sim L(\Delta/2\gamma)^{1/d}. \tag{12}$$

The product $|\Psi_\alpha(\mathbf{r}_i)|^2 |\Psi_\beta(\mathbf{r}_i)|^2$ for two states separated by ℓ has a maximal value of order $\exp[-2L(\Delta/2\gamma)^{1/d}/\xi]$, at the midpoint between the centers of localization. It follows that the second term in Eq. (11) vanishes for $L/\xi \to \infty$, in which limit the GIPR is expected to scale like the IPR.

For finite L, however, the second term in Eq. (11) introduces finite size corrections to the GIPR that make it scale differently from the conventional IPR. In order to minimize these corrections, we want to make ℓ as large as possible, which is achieved by taking γ as small as possible. We emphasize, however, that Eq. (12) only holds for $\gamma \gtrsim \Delta$, and that w_α is independent of γ when $\gamma \ll \Delta$, namely

$$\lim_{\gamma \to 0} w_\alpha = \frac{E_\alpha^{-2}}{\sum_\beta E_\beta^{-2}}. \tag{13}$$

In other words, ℓ ceases to increase when γ is much less than Δ. Our analysis therefore suggests that one cannot do much better at minimizing finite size effects than by taking $\gamma \sim \Delta$.

Finally, having established that $G_2(0)$ is determined by the first term in Eq. (11) when $L/\xi \gg 1$, we show that the weighting terms do not affect the GIPR scaling in this limit. We write $I_{2,\alpha} \approx I_2(E_\alpha)$, where $I_2(E)$ is a slowly varying function of E near $E = 0$, so that

$$G_2(0) \approx I_2(0) \sum_\alpha w_\alpha^2. \tag{14}$$

For $\gamma \gtrsim \Delta$, we may estimate the sum over eigenstates by

$$\sum_\alpha w_\alpha^2 \approx \frac{\Delta^{-1} \int dE (E^2 + \gamma^2)^{-2}}{\left[\Delta^{-1} \int dE (E^2 + \gamma^2)^{-1}\right]^2} \propto \frac{\Delta}{\gamma}. \tag{15}$$

Taking $\gamma \propto N_s^{-1}$ eliminates the L-dependence of the weighting factors in Eq. (11).

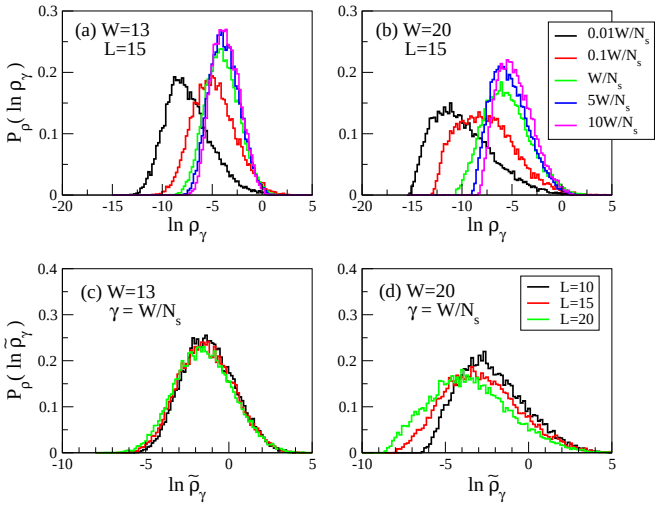

FIG. 2: (Color online) Probability distribution of the logarithm of the local density of states at $\omega = 0$. The effect of γ on $P_\rho(\ln \rho_\gamma)$ is shown for (a) extended and (b) localized states for a fixed system size. The effect of system size on $P_\rho(\ln \tilde{\rho}_\gamma)$ is shown for (c) extended and (d) localized states for $\gamma = W/N_s$. Here, $\tilde{\rho}_\gamma$ is the normalized LDOS, $\tilde{\rho}_\gamma \equiv \rho_\gamma / \langle \rho_\gamma \rangle$, where $\langle \rho_\gamma \rangle$ is the system-averaged LDOS at $\omega = 0$. Results are shown for 16 ($L = 10$), 5 ($L = 15$), and 2 ($L = 20$) disorder configurations, such that the number of LDOS values in each case is roughly the same.

In summary, we have shown that the GIPR will reproduce the scaling of the IPR in the limits of vanishingly weak and strong disorder. Moreover, we have shown that using smaller γ values to calculate the GIPR is preferable, down to $\gamma \sim \Delta$. Many numerical methods converge faster for larger γ and, for these, $\gamma \sim \Delta$ will be optimal. In the next section, we examine whether the finite size effects near W_c limit our ability to extract the critical behaviour.

III. RESULTS

We plot, in Fig. 2, the probability distribution of the logarithm of the LDOS at $\omega = 0$ for different values of γ and for different system sizes. Figures 2(a) and (b) show that γ affects both the peak position and shape of the distribution. In particular, the peak position of the distribution $P_\rho(\ln \rho_\gamma)$ is proportional to γ for $\gamma \lesssim W/N_s$, in accordance with Eq. (8). For $\gamma \gtrsim W/N_s$, the peak position and width are weak functions of γ.

In Figs. 2(c) and (d), we show the L-dependence of the distribution of the normalized LDOS, $\tilde{\rho}_\gamma \equiv \rho_\gamma / \langle \rho_\gamma \rangle$ with $\langle \rho_\gamma \rangle$ the sample-averaged density of states. Schubert et al.[28] showed that the scaling of the distribution $P_\rho(\ln \tilde{\rho}_\gamma)$ can be used to distinguish localized and extended states: $P_\rho(\ln \tilde{\rho}_\gamma)$ shifts to the left with increasing L for localized states, and is independent of L for extended states. Here, we find that there is indeed a pronounced shift for the localized case ($W = 20$), and that the distribution is

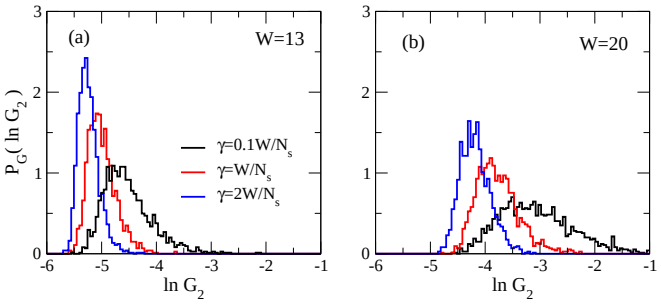

FIG. 3: (Color online) Effect of γ on the probability distribution of the GIPR at $\omega = 0$. Results are for (a) extended ($W = 13$) and (b) localized ($W = 20$) states, and are for 1500 disorder configurations with $L = 10$.

almost independent of L for the extended case ($W = 13$). The small leftward shift seen in the extended case is presumably due to finite-size effects, which are more pronounced here than in Ref. 28. Despite its smallness, this leftward shift is problematic because it obscures the signature of the Anderson transition in $P_\rho(\ln \rho_\gamma)$. This is a potentially important issue for many-body calculations where accessible system sizes tend to be severely limited. It appears that, as with other measures of localization, the usefulness of the LDOS distribution will depend on the inclusion of finite-size corrections.

Figure 3 shows the probability distribution function $P_G(\ln G_2)$ for the GIPR, obtained by calculating $G_2(\omega)$ at $\omega = 0$ for 1500 distinct impurity configurations. This figure shows that the width of the distribution depends strongly on γ, and that $P_G(\ln G_2)$ is sharply peaked when $\gamma \gtrsim \Delta$. Because the distribution of $\ln G_2$ is narrow, the mean and most probable values of the distribution are close to each other. For this reason we study the finite size scaling of the *typical* GIPR[36]

$$G_2^{\rm typ}(\omega) = \exp\left[\langle \ln G_2(\omega) \rangle\right], \qquad (16)$$

where $\langle \ldots \rangle$ refers to an average over disorder configurations.

We argued in the previous section that one should take $\gamma \propto \Delta$, where Δ depends on both N_s and W. To understand whether the W-dependence of Δ is important, we take two cases: $\gamma \propto W/N_s$ and $\gamma \propto W_c/N_s$, where W_c here refers to the accepted value of 16.5. As we discussed in Sec. II, the first choice overestimates the W-dependence of Δ, while the second choice underestimates it. Note that there is nothing fundamental about the proportionality constant W_c in the second case; it was chosen because it gives γ values that are quantitatively close to those in the first case. In total, we have taken four cases: two with $\gamma \propto W/N_s$ ($\gamma = W/N_s$ and $\gamma = 2W/N_s$) and two with $\gamma \propto W_c/N_s$ ($\gamma = W_c/N_s$, and $\gamma = 2W_c/N_s$).

Figure 4(a) shows the dependence of $G_2^{\rm typ}(0)$ on L for different strengths of disorder for the case $\gamma = W/N_s$. At short length scales, all the systems are in the critical region (albeit in a region where finite size corrections

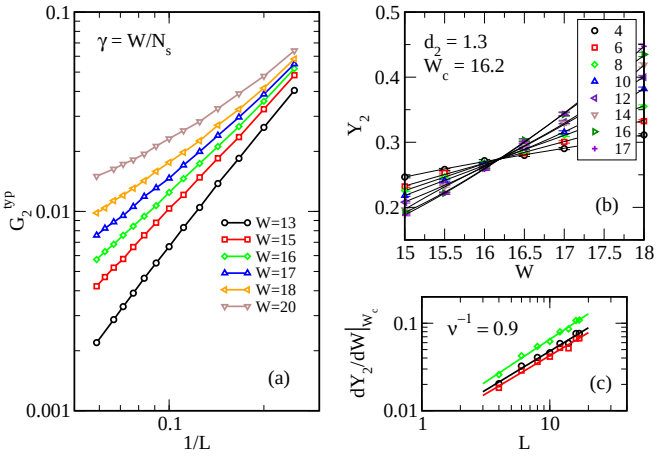

FIG. 4: (Color online) Scaling of the GIPR for $\gamma = W/N_s$. (a) Plots of $G_2^{\rm typ}$ as a function of L for 3000 disorder configurations. (b) Y_2, defined by Eq. (18), for best fit values of A_0, d_2 and y. For these parameters, the critical disorder at which all curves cross is $W_c = 16.2$, corresponding to the optimized fitting parameters $A_0 = 0.64$, $y = 1.6$, and $d_2 = 1.3$. (c) Plot of dY_2/dW at $W = W_c$ (symbols), along with power law fits (solid lines) to the data. The exponents in the fitted curves give ν^{-1}, from Eq. (20). The two outlying curves are for the extremal values $(d_2, W_c, y) = (1.5, 15.9, 3.2)$ and $(1.2, 16.4, 1.2)$ and are used to determine uncertainties for ν. The middle curve is for the optimized parameters, from which we obtain $\nu = 1.1$. Results are summarized in Table I.

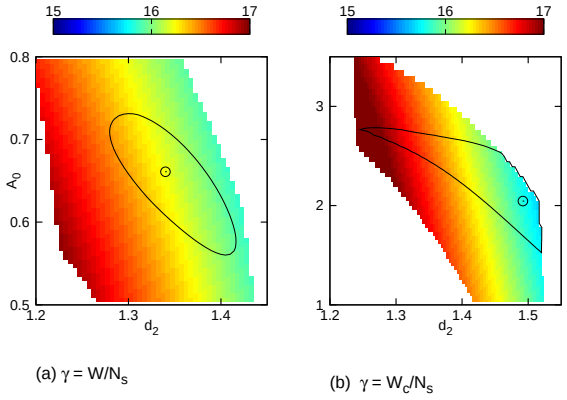

FIG. 5: (Color online) Critical parameters for (a) $\gamma = W/N_s$ and (b) $\gamma = W_c/N_s$ at the best-fit values (a) $y = 1.6$ and (b) $y = 2.9$. Intensity scale shows the value of W_X that minimizes χ^2 locally for each d_2 and A_0. Circles indicate best-fit values of d_2 and A_0, obtained from the global minimum of χ^2. Black contours bound the regions $\chi^2_{\rm red} < 1$.

are significant), and therefore all show similar size dependence. At long length scales, however, the lines diverge. For $W < W_c$, the slope becomes steeper with increasing L, consistent with a crossover to L^d with $d = 3$. For $W > W_c$, the slope decreases with increasing L, consistent with a crossover to a constant value. This figure suggests that the GIPR is indeed able to distinguish localized and extended states, even for the relatively small systems studied here.

We show that the GIPR displays the same critical behaviour as the IPR near W_c, namely that

$$G_2^{\rm typ} = L^{-d_2}\left(F\left[(W - W_c)L^{1/\nu}\right] + \frac{A_0}{L^y} + \frac{A_1}{L^{2y}} + \ldots\right) \tag{17}$$

where A_j are finite size corrections and y is the critical exponent for the leading-order irrelevant variable.[35] In all cases, we are able to obtain good scaling behaviour for $4 \le L \le 17$ with $A_j = 0$ for $j \ge 1$. We thus have five fitting parameters: d_2, W_c, ν, A_0, and y.

We now describe the fitting procedure, using the case $\gamma = W/N_s$ as an example. Figure 4(b) shows a plot of

$$Y_2 \equiv G_2^{\rm typ} L^{d_2} - \frac{A_0}{L^y} \tag{18}$$

versus W for the optimal values of A_0, y, and d_2. Error bars on the data are the root-mean-square uncertainty in $G_2^{\rm typ}$ due to the finite width of the GIPR distributions (shown, e.g., in Fig. 3). The solid curves in Fig. 4(b) are cubic fits to the data points. Each pair of curves crosses at a different disorder strength, denoted $W_j \pm \delta W_j$, where $j \in [1, N_{\rm cross}]$ and $N_{\rm cross}$ is the the number of such crossing points. (For the 8 curves shown in Fig. 4(b), there are $N_{\rm cross} = 28$ crossing points.) The uncertainties δW_j are calculated from the uncertainties in the fitting parameters. If the scaling form Eq. (17) holds and the critical parameters are correctly chosen, all curves will cross at a single point, W_X. For each A_0, y and d_2, we find $W_X(A_0, d_2, y)$ by minimizing

$$\chi^2 = \sum_{j=1}^{N_{\rm cross}} \left(\frac{W_j - W_X}{\delta W_j}\right)^2. \tag{19}$$

Plots of $W_X(A_0, d_2, y)$ are shown in Fig. 5 for optimal values of y for $\gamma = W/N_s$ and for $\gamma = W_c/N_s$. We extract our own best-fit values for W_c from the global minima of $\chi^2(A_0, d_2, y)$, and these are shown as circles in Fig. 5. A qualitative sense of the goodness-of-fit can be obtained from Fig. 4(b), which is based on the best-fit parameters for $\gamma = W/N_s$. A quantitative measure of goodness-of-fit can be obtained from the reduced chi-square $\chi^2_{\rm red} \equiv \chi^2/(N_c - 1)$. Figure 5 shows contours around the region of parameter space $\chi^2_{\rm red} < 1$. In this region, all $Y_2(W)$ curves cross, within error, at a common point.

The best-fit values for W_c and d_2 are summarized in Table I, along with previously published values. Quantities in brackets are extremal parameter values satisfying $\chi^2_{\rm red} < 1$, and are used to estimate the uncertainty in the critical parameters. The values for W_c and d_2 found from this analysis are generally within uncertainty of the previously published results.

γ	d_2	W_c	ν	y
W/N_s	1.3 (1.2,1.5)	16.2 (15.9,16.4)	1.1 (1.0,1.1)	(1.2,3.2)
$2W/N_s$	1.3 (1.0,1.4)	16.6 (15.9,17.2)	1.0 (0.9,1.4)	(1.4,2.5)
W_c/N_s	1.5 (1.2,1.5)	15.8 (15.7,17.0)	1.3 (1.3,1.4)	(2.1,3.0)
$2W_c/N_s$	1.1 (1.0,1.4)	17.2 (16.2,17.4)	1.7 (1.2,1.8)	(1.7,2.2)
published	1.3	16.54	1.57	

TABLE I: Critical parameters from finite-size scaling. For comparsion, previously published results from Ref. 35 and Ref. 31 are shown. In the first column, W_c refers to the accepted value of 16.5. Numbers in parenthesis are estimated bounds on parameters, and are based on the parameter regions $\chi^2_{\rm red} \leq 1$.

The next step is to obtain the critical exponent ν, which is done by fitting a power law to

$$\left.\frac{dY_2}{dW}\right|_{W=W_c} = L^{1/\nu} F'(0). \qquad (20)$$

In Fig. 4(c), we show dY_2/dW at $W = W_c$, along with power law fits to the data. The three curves correspond to the best-fit, minimal, and maximal values of W_c and d_2 shown in Table I. The fitted exponents give three values of ν for each γ, and are shown in the fourth column of Table I. We note that ν is systematically underestimated for $\gamma \propto W/N_s$, but is closer to the correct answer for $\gamma \propto W_c/N_s$. One of the conclusions of this work is that ν is more sensitive to the W-dependence of γ than either W_c or d_2. This follows directly from the derivative with respect to W in Eq. (20), and means that obtaining an accurate value for ν depends on establishing an accurate relationship between Δ and W.

In summary, we have shown that the GIPR can distinguish between localized and extended states, and moreover that it is possible to extract critical parameters from a scaling analysis of the GIPR. The main issue which arises is how the broadening γ influences the results. In Table I, comparing $\gamma = 2W/N_s$ with $\gamma = W/N_s$ and comparing $\gamma = 2W_c/N_s$ with $\gamma = W_c/N_s$, we see that the results for larger γ generally have larger uncertainties, but do not appear to be systematically shifted towards or away from their true values. It thus seems likely that one could obtain accurate values of W_c and d_2 for larger values of γ provided one can study systems that are large enough to keep the uncertainties to a reasonable size. As mentioned above, one has the additional requirement that γ and Δ both have the same dependence on W in order obtain accurate values for ν. This can be achieved, for example, by taking $\gamma \propto 1/\rho_0(W)N_s$, where $\rho_0(W)$ is the ensemble-averaged density of states calculated for each strength of disorder.

IV. CONCLUSIONS

We have tested the usefulness of a generalized inverse participation ratio as a measure of Anderson localization by benchmarking it against the well-studied case of a disordered three-dimensional tight binding lattice. Because the generalized inverse participation ratio depends on the local density of states, and not the single particle wavefunctions, it is potentially useful for studying interacting systems where single particle wavefunctions are not defined. We have found that it is possible to extract critical parameters for the Anderson MIT, and have shown that finite size effects are not an impediment if the spectral broadening γ used to calculate the local density of states is of the same order as the level spacing Δ.

Acknowledgments

We acknowledge the support of NSERC of Canada. This work was made possible by the facilities of the Shared Hierarchical Academic Research Computing Network (SHARCNET).

* Electronic address: billatkinson@trentu.ca

[1] P. W. Anderson, Phys. Rev. **109**, 1492 (1958).
[2] P. A. Lee and T. V. Ramakrishnan, Rev. Mod. Phys. **57**, 287 (1985).
[3] B. L. Altshuler and A. G. Aronov, in *Electron-electron interactions in disordered systems*, edited by A. L. Efros and M. Pollak (North Holland, New York, 1985), vol. 10 of *Modern Problems in Condensed Matter Sciences*.
[4] E. Abrahams, S. V. Kravchenko, and M. P. Sarachik, Rev. Mod. Phys. **73**, 251 (2001).
[5] A. Punnoose and A. M. Finkelstein, Science **310**, 289 (2005).
[6] I. Gornyi, A. Mirlin, and D. Polyakov, Phys. Rev. Lett. **95**, 206603 (2005).
[7] D. Basko, I. Aleiner, and B. Altshuler, Annals of Physics **321**, 1126 (2006).
[8] E. Miranda and V. Dobrosavljević, Rep. Prog. Phys. **68**, 2337 (2005).
[9] D. Tanasković, V. Dobrosavljević, E. Abrahams, and G. Kotliar, Phys. Rev. Lett. **91**, 066603 (2003).
[10] D. Heidarian and N. Trivedi, Phys. Rev. Lett. **93**, 126401 (2004).
[11] P. B. Chakraborty, P. J. H. Denteneer, and R. T. Scalettar, Phys. Rev. B **75**, 125117 (2007).
[12] P. Henseler, J. Kroha, and B. Shapiro, Phys. Rev. B **77**, 075101 (2008).
[13] Y. Song, R. Wortis, and W. A. Atkinson, Phys. Rev. B **77**, 054202 (2008).
[14] P. Henseler, J. Kroha, and B. Shapiro, Phys. Rev. B **78**, 235116 (2008).
[15] K. Byczuk, W. Hofstetter, and D. Vollhardt, Phys. Rev. Lett. **94**, 056404 (2005).

[16] D. Semmler, K. Byczuk, and W. Hofstetter, Phys. Rev. B **81**, 115111 (2010).
[17] H. Shinaoka and M. Imada, J. Phys. Soc. Jpn. **78**, 094708 (2009).
[18] Y. P. Chen, J. Hitchcock, D. Dries, M. Junker, C. Welford, and R. G. Hulet, Phys. Rev. A **77**, 033632 (2008).
[19] L. Fallani, J. E. Lye, V. Guarrera, C. Fort, and M. Inguscio, Phys. Rev. Lett. **98**, 130404 (2007).
[20] M. White, M. Pasienski, D. McKay, S. Q. Zhou, D. Ceperley, and B. DeMarco, Phys. Rev. Lett. **102**, 055301 (2009).
[21] B. Deissler, M. Zaccanti, G. Roati, C. D'Errico, M. Fattori, M. Modugno, G. Modugno, and M. Inguscio, Nat. Phys. **6**, 354 (2010).
[22] G. Modugno, Reports on Progress in Physics **73**, 102401 (2010).
[23] M. Janssen, Physics Reports **295**, 1 (1998).
[24] V. Dobrosavljević, A. A. Pastor, and B. K. Nikoli, Europhysics Letters **62**, 76 (2003).
[25] Y. Song, W. A. Atkinson, and R. Wortis, Phys. Rev. B **76**, 045105 (2007).
[26] R. Wortis, Y. Song, and W. A. Atkinson, Physica B **403**, 1468 (2008).
[27] M.-T. Tran, Phys. Rev. B **76**, 245122 (2007).
[28] G. Schubert, J. Schleede, K. Byczuk, H. Fehske, and D. Vollhardt, Phys. Rev. B **81**, 155106 (2010).
[29] A. Rodriguez, L. J. Vasquez, K. Slevin, and R. A. Römer, Phys. Rev. Lett. **105**, 046403 (2010).
[30] A. D. Mirlin, Physics Reports **326**, 259 (2000).
[31] A. Mildenberger, F. Evers, and A. D. Mirlin, Phys. Rev. B **66**, 033109 (2002).
[32] J. Brndiar and P. Markos, Phys. Rev. B **74**, 153103 (2006).
[33] R. Haydock and R. L. Te, Phys. Rev. B **49**, 10845 (1994).
[34] A. MacKinnon and B. Kramer, Phys. Rev. Lett. **47**, 1546 (1981).
[35] K. Slevin and T. Ohtsuki, Phys. Rev. Lett. **82**, 382 (1999).
[36] A. D. Mirlin and F. Evers, Phys. Rev. B **62**, 7920 (2000).